

Development and validation of a new cloud simulation experiment for lab-based aerosol–cloud studies

Cite as: Rev. Sci. Instrum. **93**, 095106 (2022); <https://doi.org/10.1063/5.0098777>

Submitted: 12 May 2022 • Accepted: 26 August 2022 • Published Online: 30 September 2022

 F. Vogel, L. Lacher, J. Nadolny, et al.



View Online



Export Citation



CrossMark

ARTICLES YOU MAY BE INTERESTED IN

[Active impedance matching of a cryogenic radio frequency resonator for ion traps](#)

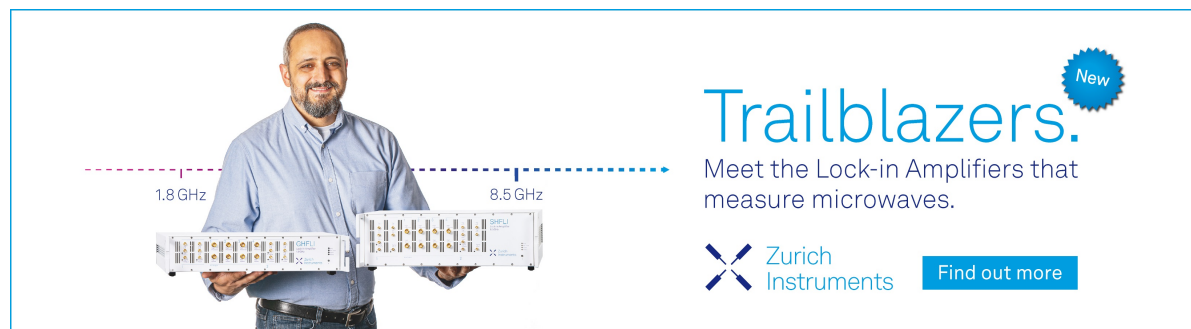
Review of Scientific Instruments **93**, 093201 (2022); <https://doi.org/10.1063/5.0097583>


[Use of a Mylar filter to eliminate vacuum ultraviolet pulse pileup in low-energy x-ray measurements](#)

Review of Scientific Instruments **93**, 093531 (2022); <https://doi.org/10.1063/5.0101712>


[Three-dimensional hot-spot x-ray emission tomography from cryogenic deuterium–tritium direct-drive implosions on OMEGA](#)

Review of Scientific Instruments **93**, 093530 (2022); <https://doi.org/10.1063/5.0098977>



Trailblazers. 

Meet the Lock-in Amplifiers that measure microwaves.

 Zurich Instruments [Find out more](#)

Development and validation of a new cloud simulation experiment for lab-based aerosol–cloud studies

Cite as: Rev. Sci. Instrum. 93, 095106 (2022); doi: 10.1063/5.0098777

Submitted: 12 May 2022 • Accepted: 26 August 2022 •

Published Online: 30 September 2022





View Online



Export Citation



CrossMark

F. Vogel,  L. Lacher, J. Nadolny, H. Saathoff,  T. Leisner,  and O. Möhler^{a)} 

AFFILIATIONS

Institute of Meteorology and Climate Research, Karlsruhe Institute of Technology, Hermann-von-Helmholtz-Platz 1, 76344 Eggenstein-Leopoldshafen, Germany

^{a)} Author to whom correspondence should be addressed: ottmar.moehler@kit.edu

ABSTRACT

The Aerosol Interaction and Dynamics in the Atmosphere (AIDA) cloud expansion chamber with a volume of 84 m³ was extended for the small cloud expansion chamber AIDA mini (AIDAm) with a volume of 20 L. AIDAm is located in the cold room of AIDA and can perform automated ice-nucleation measurements over longer time periods of hours to days. AIDAm samples from the AIDA chamber, which acts as a reservoir of atmospheric aerosol types, which can slowly be modified by physical or chemical processes similar to those occurring in the atmosphere. AIDAm was validated for accurate ice-nucleation temperature control by measuring homogeneous freezing of pure water droplets at temperatures around −34 °C and for immersion freezing induced by dust aerosol particles in the temperature range between −20 and −30 °C. Further validation experiments at cirrus cloud temperatures of −45 °C revealed that AIDAm can distinguish between heterogeneous ice formation on mineral dust aerosols and homogeneous freezing of sulfuric acid solution particles. The contribution of homogeneous and heterogeneous ice formation processes to the ice-nucleation activity of coated dust particles was investigated in a 7 h long experiment, where solid dust particles were slowly coated with sulfuric acid. The continuous AIDAm measurements with a time resolution of 6 min showed a substantial suppression of the heterogeneous freezing phenomenon and an increasing role of homogeneous freezing while the coating amount was slowly increased. This experiment proved the capability of AIDAm to sensitively detect small changes in the ice-nucleation ability of aerosols, which undergo slow processing like chemical surface coating.

© 2022 Author(s). All article content, except where otherwise noted, is licensed under a Creative Commons Attribution (CC BY) license (<http://creativecommons.org/licenses/by/4.0/>). <https://doi.org/10.1063/5.0098777>

I. INTRODUCTION

Cloud simulation chambers have been used since the 1960s to investigate different processes related to atmospheric microphysics, aerosol and cloud chemistry, and cloud radiative properties under well-controlled conditions in the laboratory (Chang *et al.*, 2016). One special class is that of cloud expansion chambers, in which the contribution of certain aerosol systems to atmospheric cloud droplet and ice formation can be studied. Regardless of their size, the basic working principle of cloud expansion chambers is based on adiabatic cooling induced by a controlled pressure reduction inside the cloud chamber. The decreasing temperature causes the ice and water saturation ratio (S_{ice} and S_{water} , respectively) to increase and to reach values larger than 1, where the air is supersaturated and liquid cloud droplets and ice crystals can form.

Depending on the temperature and saturation conditions inside the cloud chamber, ice crystals form through different freezing mechanisms. For mixed-phase cloud conditions, at temperatures between 0 and −35 °C, the predominant freezing pathway is the immersion freezing in which an aerosol particle is immersed in a supercooled liquid cloud droplet and then triggers the ice formation (e.g., de Boer *et al.*, 2011; Hoose and Möhler, 2012; Vali *et al.*, 2015; and Kanji *et al.*, 2017). In pure ice clouds, the so-called cirrus clouds, at temperatures below the homogeneous freezing temperature of water at −35 °C, primary ice formation is either induced by deposition ice nucleation, where water vapor freezes directly on the aerosol particles (Vali *et al.*, 2015) or the pore condensation and freezing mechanism, where it is assumed that water condenses in capillaries of porous aerosol particles and freezes upon further cooling (e.g., Wagner *et al.*, 2016; David *et al.*, 2019; and Marcolli, 2020).

Atmospheric aerosol particles contributing to ice formation are called ice-nucleating particles (INPs) (e.g., Pruppacher and Klett, 2010; Hinds, 2012; Vali *et al.*, 2015; and Seinfeld and Pandis, 2016). Many laboratory studies have been performed to investigate the freezing ability of different aerosol types, such as soil dust, soot, organic materials, primary biological particles, secondary organic aerosols (SOAs), and sulfuric acid for different temperature regimes (e.g., Hiranuma *et al.*, 2015; Wex *et al.*, 2015; Ignatius *et al.*, 2016; and Ullrich *et al.*, 2017). In particular, dust particles turned out to be good INPs in both the mixed-phase and cirrus cloud regime (e.g., Chou *et al.*, 2011; Atkinson *et al.*, 2013; Kanji *et al.*, 2017; and Boose *et al.*, 2019), triggering ice formation at even low S_{ice} values. Compared to dust, aerosol particles such as SOA particles show a less pronounced heterogeneous ice-nucleation ability (e.g., Ignatius *et al.*, 2016; Wolf *et al.*, 2020), and higher S_{ice} values, much closer to the homogeneous freezing conditions need to be reached to induce heterogeneous ice formation. Materials such as sulfuric acid solution droplets (H_2SO_4) freeze homogeneously at a temperature of $-35^\circ C$ or lower (e.g., Koop *et al.*, 2000; Schneider *et al.*, 2021b).

Atmospheric aerosol particles stem from many different sources distributed around the globe. Depending on their size, they are then lifted from ground level to upper tropospheric regions (e.g., Knippertz and Todd, 2012). Once the aerosol particles reach higher levels in the atmosphere, they can be transported over distances of up to a few thousand kilometers away from their emission source (e.g., Betzer *et al.*, 1988; Weinzierl *et al.*, 2017) and remain in the atmosphere for up to several days or weeks. During their residence time in the atmosphere, aerosol particles can interact with each other by coagulation or gaseous materials can condense on the surface of solid particles. These physical and chemical aging processes may change the ice-nucleation ability of the unprocessed aerosol and eventually lead to a different predominant freezing mechanism.

One type of atmospheric aging process is the coating of solid aerosol particles with gaseous material. In the last 15 years, studies (e.g., Cziczo *et al.*, 2009; Möhler *et al.*, 2008; and Knopf and Koop, 2006) have investigated the influence of SOA and H_2SO_4 coatings on different aerosol particles at cirrus cloud conditions with temperatures between -34 and $-60^\circ C$. The relative humidity with respect to ice at which the ice formation was observed to set-in was about 40% higher for the coated dust aerosol than for the non-coated dust aerosol. This clearly shows a suppression of the heterogeneous ice formation potential of the pure dust by the SOA or H_2SO_4 surface coating layer.

However, in most of the studies mentioned above, the particles were coated at room temperature in an external vessel and then transferred to the instruments measuring the ice-nucleating properties. This does not necessarily represent atmospheric conditions, where the coating may also occur at lower temperatures during transport through the middle and upper troposphere. Furthermore, the H_2SO_4 coating was often applied using hot sulfuric acid vapor with a temperature of about $150^\circ C$. The high temperature may induce chemical reactions that could modify the properties of the dust particles and thus also influence their ice-nucleating properties. For further studies, it is, therefore, important to coat the particles in a wide range of atmospherically relevant conditions and measure their ice-nucleating properties

at relevant atmospheric conditions during the ongoing coating process.

The small AIDAm (Aerosol Interaction and Dynamics in the Atmosphere mini) expansion-type cloud chamber was developed for use in combination with the existing AIDA (Aerosol Interaction and Dynamics in the Atmosphere) cloud chamber facility. While AIDA provides a wide range of well-controlled temperature, pressure, and humidity conditions for atmospheric aerosol and cloud experiments, AIDAm can monitor the ice-nucleation ability of the aerosol inside AIDA under the same conditions. Depending on the particle size, aerosols can reside in the AIDA aerosol chamber for several days or even a week without substantial loss (e.g., Saathoff *et al.*, 2001; 2003; and Schnaiter *et al.*, 2005), which comes close to typical atmospheric aerosol residence times. Therefore, the approach combining AIDAm and AIDA makes use of the unique feature of AIDA for long-term physical and chemical aging of atmospheric aerosols at typical atmospheric thermodynamic conditions, concentrations, and residence times and the capabilities of the new AIDAm chamber for measuring the impact of the ongoing aging processes on the ice-nucleating properties of the aerosols at high sensitivity and time resolution. In the following, we describe the setup and working principle of the new cloud chamber AIDAm and show the results from the validation experiments at both mixed-phase and cirrus cloud conditions.

II. METHODS

A. The AIDA cloud chamber

The Aerosol Interaction and Dynamics in the Atmosphere (AIDA) cloud simulation chamber has been used for about 20 years for investigating the ice-nucleation properties of atmospheric aerosols. The cloud chamber (Fig. 1, left) described in detail by, e.g., Möhler *et al.* (2003; 2006) or Wagner *et al.* (2006) has a volume of about 84 m^3 and is placed inside a thermal housing, in which the temperature can be regulated over a wide range from 60 to $-90^\circ C$. The pressure inside the chamber can be controlled to values from about 1000 mbar to below 1 mbar . The total water concentration is measured with a dew point mirror (373LX, MBW), and the gas-phase water concentration in the presence and absence of clouds is measured with two tunable diode laser spectrometers, viz., SpAPicT (Single Path AIDA PCI in-cloud Tunable Diode Laser) and APicT (AIDA PCI in-cloud Tunable Diode Laser) (Fahey *et al.*, 2014).

The mineral dust aerosol investigated in this work was generated by dispersing a bulk sample with a rotating brush generator (RBG 1000, Palas GmbH). The aerosol flow from the RBG 1000 was passed through two cyclone impactors to remove particles with a diameter larger than about $5\text{ }\mu\text{m}$ and was then added to the AIDA chamber.

The aerosol number concentration was measured with a condensation particle counter (CPC 3010, TSI Inc.) and the aerosol size distribution was obtained from the combined measurements with a scanning mobility particle sizer (SMPS: DMA, 3071; CPC, 3772, both TSI Inc.) and an aerodynamic particle spectrometer (APS 3021, TSI Inc.). Two optical particle counters (OPCs, welas2000, Palas GmbH, see Sec. II B 1 for a detailed description) are located in the thermal housing below the cloud chamber and are connected to it with vertical sampling lines. Each OPC takes a sample flow of

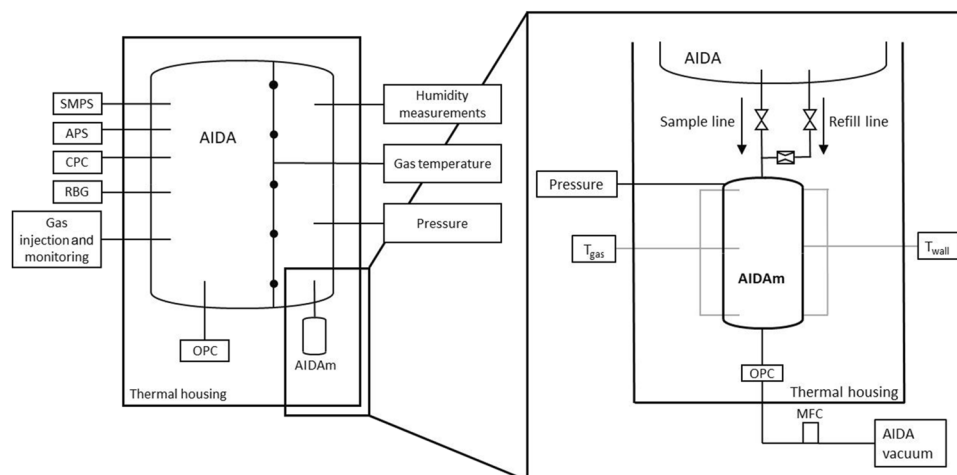


FIG. 1. Schematic (not to scale) of the AIDAm cloud expansion chamber (right part) located in the temperature-controlled housing of the AIDA cloud chamber (left part).

5 L min⁻¹ to measure the number concentration of large aerosol particles, liquid cloud droplets, and ice crystals in different size ranges of 0.7–46 μm (welas 2300 sensor) and 5–240 μm (welas 2500 sensor) (Wagner *et al.*, 2016).

B. The small expansion chamber AIDAm

The large volume and the long preparation time for experiments limit the operation of the AIDA cloud chamber to a few cloud expansion experiments per day. Therefore, the much smaller cloud expansion chamber AIDAm, described in detail in the following, was developed. It is located in the thermal housing of AIDA for repeated cloud expansion experiments with a turnover time between the single cloud expansions of only 5–7 min. AIDAm samples air from the AIDA chamber, which serves as a reservoir of aerosols with only slowly changing number concentrations and size distributions (see Sec. III A). This way, AIDAm can monitor, e.g., changes in the ice-nucleation ability of aerosol particles slowly modified by physical or chemical aging processes over longer time periods inside AIDA.

1. Setup of AIDAm

The construction of AIDAm was inspired by the Portable Ice-Nucleation Experiment, PINE (Möhler *et al.*, 2021), which is a small and mobile cloud expansion chamber for ice-nucleation studies and atmospheric INP measurements. Similar to PINE, AIDAm consists of a cloud chamber, a particle detector, and a control system for automated operation. However, it does not need a cooling system because the cloud chamber is located inside the thermal housing of the AIDA chamber (Fig. 1). With a volume of 20 L, a height of 60 cm, and a diameter of 25 cm, the AIDAm cloud chamber is about twice as large as the PINE cloud chamber. It is connected to the AIDA cloud chamber with two vertical stainless steel tubes (sample line and refill line) for sampling and investigating aerosols at temperature and humidity conditions that are controlled by the AIDA cloud chamber system as described in Sec. II A.

The wall temperature (T_{wall}) of the AIDAm chamber is measured with three thermocouples attached to the outer wall at the top, the middle, and the bottom of the cloud chamber. The gas

temperature (T_{gas}) inside the cloud chamber is measured with three additional thermocouples, located about 5 cm off the wall and at about 5, 30, and 55 cm above the bottom of the chamber. Thus, they are positioned close to the wall temperature sensors. The pressure in the AIDAm chamber is measured with a pressure sensor (VSC43MV, Thyracont).

The flow rate through AIDAm is controlled with a mass flow controller (MFC) that is connected to the AIDA vacuum system. The gas flow from the chamber passes an OPC, located below the chamber. It detects the size of the different types of particles that can be present in the AIDAm chamber, viz., nonactivated aerosol particles, liquid cloud droplets, and ice crystals. The OPC is a welas 2500 sensor connected to a Promo[®] 2000 control unit (Palas GmbH). The welas sensor uses white light and detects the light scattered by individual particles at a range of scattering angles around 90°. Particles crossing the detection volume scatter the light in a size and shape-dependent way, such that aspherical particles show a higher intensity of the scattered light than spherical particles with the same volume. This way, ice crystals can be distinguished from liquid cloud droplets because of their larger optical size (Järvinen *et al.*, 2014).

2. Working principle

AIDAm is operated in a similar way as PINE (Möhler *et al.*, 2021), in which sequences of runs and operations are performed. Thereby, an operation consists of a series of consecutively performed runs, where each run has three modes: flush, expansion, and refill.

In the flush mode, the AIDAm chamber is flushed with air from the AIDA chamber, containing the aerosol particles under investigation. As shown in the upper panel of Fig. 2, the pressure (black line) and the temperature (blue line) inside the chamber are constant. Only the larger aerosol particles are detected in the size range of the OPC (Fig. 2, lower panel). Each point represents one particle with its optical diameter d calculated from the detected size-dependent scattering intensity. Typical settings for the flush mode are a constant volume flow between 5 and 10 L min⁻¹ for a time between 2 and 4 min (see Table I). Thus, the AIDAm chamber is filled with fresh aerosol from AIDA.

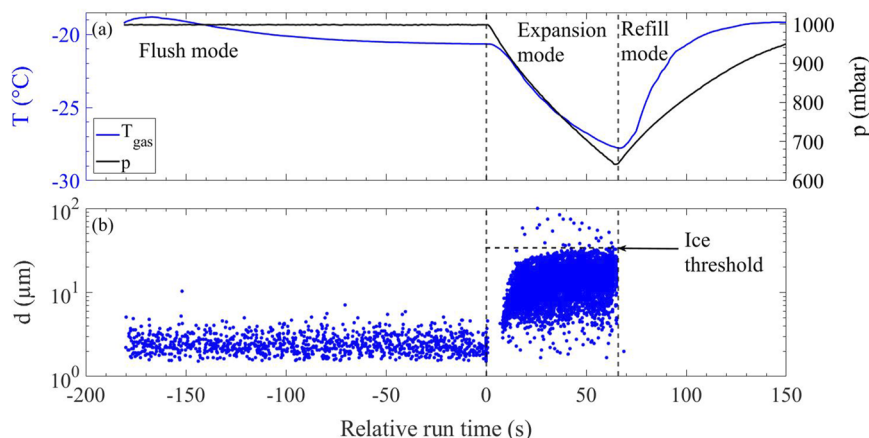


FIG. 2. Single run of an AIDAm expansion including the flush mode, the expansion mode, and the refill mode. Panel (a) shows in black the pressure and in blue the gas temperature measured in the AIDAm chamber. (b) Single particle data from the OPC, where each point represents the optical diameter of one detected particle. In the flush mode, only large aerosol particles are detected. During the expansion, a liquid cloud forms (seen as an accumulation of many data points), and ice crystals are detected as larger particles above the liquid cloud.

The flush mode is followed by the expansion mode, which is initiated by closing the valve in the sample line between AIDA and AIDAm. A constant expansion flow, with values between 5 and 10 L min⁻¹, is applied to steadily reduce the chamber pressure from the start pressure, which is equal to the AIDA cloud chamber pressure, to the end pressure between 900 and 750 mbar. The decrease in pressure induces a decrease in temperature due to expansion cooling, which can be seen in the upper panel of Fig. 2, and an increase in saturation with respect to ice and water, yielding supersaturated conditions. The expansion starts at a relative run time of 0 s and lasts for about 65 s in this case. The experiment presented in Fig. 2 shows the formation of a mixed-phase cloud, where both cloud droplets and ice crystals were visible in the OPC data. After about 6 s from the start of the expansion, a dense liquid cloud formed with particle diameters lower than about 35 μm and only a few ice crystals were detected as larger particles with diameters above the ice threshold of 35 μm. As shown in Eq. (1), the INP concentration is calculated from the ratio of the total number of ice crystals (ΔN_{ice}) detected during the expansion and the volume of air that passed the OPC (ΔV_{exp}) during the presence of a cloud in AIDAm. The air volume is obtained by multiplying the total time from the beginning of the cloud droplet activation until the end of the expansion (Δt_{exp}) with the constant volume flow rate during the expansion (Δf_{exp}). The correction factor of 0.105 accounts for the fact that only 10.5% of the total air volume passes the optical detection volume located in the center of the welas 2500 sampling tube,

$$INP_{AIDAm} = \frac{\Delta N_{ice}}{\Delta V_{exp} \cdot 0.105} = \frac{\Delta N_{ice}}{\Delta t_{exp} \cdot \Delta f_{exp} \cdot 0.105}. \quad (1)$$

TABLE I. Typical values for the flow, the end pressure, and the resulting duration for the three modes of a run.

Run mode	Flow (L min ⁻¹)	End pressure (mbar)	Duration (s)
Flush	5–10	...	120–240
Expansion	5–10	900 – 750	20–90
Refill	Orifice	...	40–90

The final refill mode of an AIDAm run is started by opening the valve in the refill line (see Fig. 1). A small orifice in the refill line ensures a smooth refilling of the AIDAm chamber with aerosol from the AIDA chamber. Once the chamber is refilled to the AIDA pressure, the valve in the refill line is closed, the valve in the sample line is opened, and the next run is started with the flush mode.

C. The droplet freezing experiment INSEKT

The INP measurements made with AIDAm were compared not only to the results from AIDA but also to the measurements with another INP instrument called INSEKT (Ice Nucleation Spectrometer of the Karlsruhe Institute of Technology) (Schneider *et al.*, 2021a). For this method, aerosol particles from the AIDA chamber were sampled on a nuclepore filter with a pore size of 0.4 μm and a diameter of 47 mm for a duration of 30 min, while AIDAm was sampling the same aerosol from the well-mixed AIDA cloud chamber volume. This allowed for a direct comparison of the measured INP concentrations.

For the offline INP analysis with INSEKT, the sampled aerosol particles are washed off the filter with nanopure water. The resulting suspension is diluted twice (1:15 and 1:225) and 50 μl of the undiluted suspension and the two dilutions are pipetted into the wells of two PCR plates with a total number of 160 wells. A total of 32 wells of the PCR plates are filled with nanopure water as a freezing reference. The so-prepared PCR plates are placed in the INSEKT instrument and are cooled at a rate of 0.33 K min⁻¹ and the temperature-dependent freezing behavior of the suspension in the wells is observed with a camera. From the temperature at which the single volumes froze, an INP-temperature spectrum is calculated in 0.5 °C steps following the formulation from Vali (1971).

D. Aerosol samples

For the experiments presented here, several types of aerosol were used. This section describes the aerosols used for both the AIDAm validation experiments and the experiments investigating coating effects on ice-nucleation. The coating materials and procedures will also be described.

SDSA_01: This soil dust sample originates from the Succulent Karoo biome near Soebatsfontein, a semiarid desert region in South

Africa. Sampling probes were directly collected from the soil surface, with some of them also containing biocrust (Maier *et al.*, 2018). After collection, the material was sieved for particle diameters smaller than 20 μm , such that only the portion of particles in an atmospherically relevant diameter range is left.

AS: Ammonium sulfate was injected with an ultrasonic nebulizer (GA 2400, SinapTec) into AIDA starting from a solution containing 1 wt. % of AS. The solution was then dispersed into small droplets, which were passed through a diffusion dryer. The resulting solid particles were then transferred into the AIDA chamber.

H₂SO₄: The sulfuric acid coating was obtained by the formation of sulfuric acid molecules inside the chamber, which was initiated by the reaction of SO₂ with OH radicals. The latter was formed by the dark reaction of tetramethylethylene (TME) with O₃.

III. INSTRUMENT VALIDATION

By comparison with AIDA and INSEKT results, the new AIDAm cloud expansion chamber was validated for measuring immersion freezing INPs, the correct freezing onset temperature of supercooled water droplets, and freezing processes at cirrus cloud temperatures. The immersion freezing experiments were conducted with a natural soil dust sample (SDSA_01). Dust aerosol is known to induce ice formation in the immersion freezing mode already at temperatures of about -15 to -20 °C (e.g., Hoose and Möhler, 2012; Murray *et al.*, 2012; Ullrich *et al.*, 2017; and Kanji *et al.*, 2017) and, thus, allows for comparisons in a temperature range accessible to all measuring instruments.

The experiments on homogeneous freezing of supercooled water droplets were conducted with AS particles. In the course of the expansion in AIDA or AIDAm, the AS aerosol particles acted as cloud condensation nuclei to form supercooled liquid droplets, which then froze homogeneously according to further expansion cooling. The experiments at cirrus conditions were conducted either with aqueous sulfuric acid aerosol to investigate the response of AIDAm for homogeneous freezing of solute particles or with mineral dust aerosols. The dust aerosol was used to investigate and document the transition from homogeneous freezing signals to heterogeneous ice-nucleation. Start temperatures, aerosol types, and aerosol number concentrations of the validation experiments are listed in Table II.

A. Immersion freezing

Two immersion freezing experiments were conducted to compare AIDAm with AIDA and INSEKT. The first experiment was

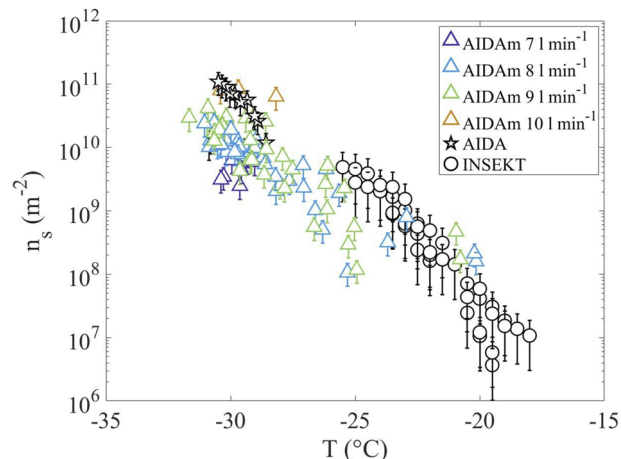


FIG. 3. Temperature-dependent INAS density, n_s , measured with AIDA (stars), AIDAm (triangles), and INSEKT (circles) for the natural soil dust sample SDSA_01. The AIDA temperature was set to -25 °C. AIDAm was operated at expansion flow rates between 7 and 10 L min⁻¹, which are represented by different colors.

performed at a constant temperature to also investigate the reproducibility of AIDAm measurements at the same settings. During the second experiment, the temperature in the thermal housing of AIDA was slowly reduced from -10 to -27 °C to obtain AIDAm results in a temperature range well overlapping with the INSEKT data. During both experiments, the aerosol particles in AIDA were also sampled on two filters for offline INP analysis with INSEKT. More than 100 AIDAm runs were conducted with various expansion flow settings between 7 and 10 L min⁻¹.

The results from the three instruments are presented in Fig. 3 as INAS (Ice Nucleation Active Surface site) densities (n_s) as a function of temperature. The n_s approach gives the number of ice active sites on the surface of the aerosol particles and is calculated as the ratio of the measured INP number concentration to the total aerosol surface area concentration (Niemand *et al.*, 2012; Ullrich *et al.*, 2017; and Schneider *et al.*, 2021a). The n_s values also allow for comparing results from experiments with different aerosol concentrations. The calculation of n_s uncertainties for AIDA and AIDAm is based on the individual uncertainties for the INP concentration and the total aerosol surface area concentration and the uncertainties are about 40%. The INSEKT measurements have an error of about 70%.

TABLE II. Summary of the AIDAm validation experiments, with the AIDA experiment temperature T_{AIDA} , the aerosol type, the aerosol number concentration $c_{\text{n,ae}}$ in the AIDA chamber, the number of AIDAm runs, and the respective ice-nucleation mode.

T_{AIDA} (°C)	Aerosol	$c_{\text{n,ae}}$ (cm ⁻³)	# AIDAm runs	Ice-nucleation mode
-25	SDSA_01	175	41	Immersion freezing
-10 to -27	SDSA_01	180	63	Immersion freezing
-31	AS	195	53	Homogeneous freezing
-45	H ₂ SO ₄	1000	10	Homogeneous freezing
-45	SDSA_01	160	18	Deposition nucleation

The n_s values measured during the AIDA expansion increased from $1 \times 10^{10} \text{ m}^{-2}$ at a temperature of -28.5°C to $1 \times 10^{11} \text{ m}^{-2}$ at -31.5°C (black stars in Fig. 3). The results from AIDAm showed up to about one order of magnitude lower n_s values compared to AIDA (colored triangles in Fig. 3). Only for the expansions with a flow of 10 L min^{-1} , AIDAm data agreed well with the AIDA data. The n_s measured with INSEKT (black circles in Fig. 3) ranged from $1 \times 10^7 \text{ m}^{-2}$ at a temperature of -18°C to $5 \times 10^9 \text{ m}^{-2}$ at -26°C and thus compared well with the AIDAm data within the given uncertainties.

Figure 4 shows a comparison of the AIDA results with the AIDAm measurements for the different expansion flow settings between 7 and 10 L min^{-1} . The best agreement between AIDA and AIDAm measurements is observed for the highest AIDAm expansion flow of 10 L min^{-1} . With a decrease in expansion flow, the deviation between AIDA and AIDAm increased to a factor of up to 5, 10, and 15 for the respective expansion flows of 9, 8, and 7 L min^{-1} . This increasing deviation may be caused by a smaller fraction of aerosol particles being activated as supercooled cloud droplets at lower expansion flow rates and thus a smaller fraction of the aerosol available to induce immersion freezing. This leads to an underestimation of n_s . During an AIDA experiment, the number concentration of cloud droplets is measured and it reveals that almost all aerosol particles are activated as supercooled cloud droplets, which then contribute to immersion freezing.

The reproducibility of AIDAm measurements was investigated for an expansion flow of 9 L min^{-1} over a time period of several hours. The experiment was started with a concentration of 200 cm^{-3} of the SDSA_01 aerosol sample in AIDA, and over a time of 5 h, AIDAm runs were performed with the same settings during three short time intervals. As shown in the lower panel of Fig. 5, the aerosol concentration in AIDA only slowly decreased from the initial concentration to about 175 cm^{-3} due to settling losses inside the chamber, but it showed no short-term fluctuations. These rather constant aerosol conditions can be maintained in AIDA

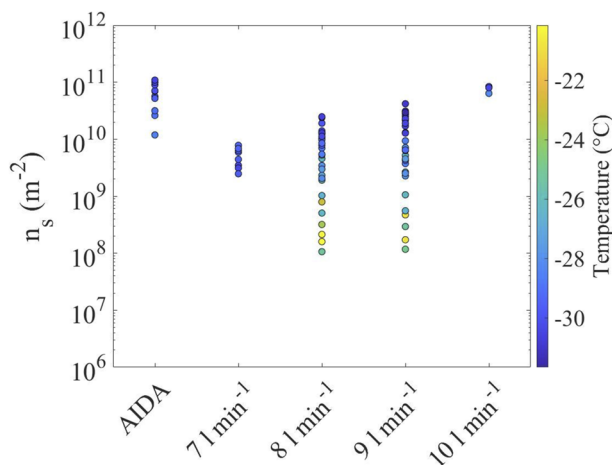


FIG. 4. Comparison of n_s values measured with AIDAm expansion flow rates of 7, 8, 9, and 10 L min^{-1} , and measured with AIDA. The color bar represents the respective ice-nucleation temperature.

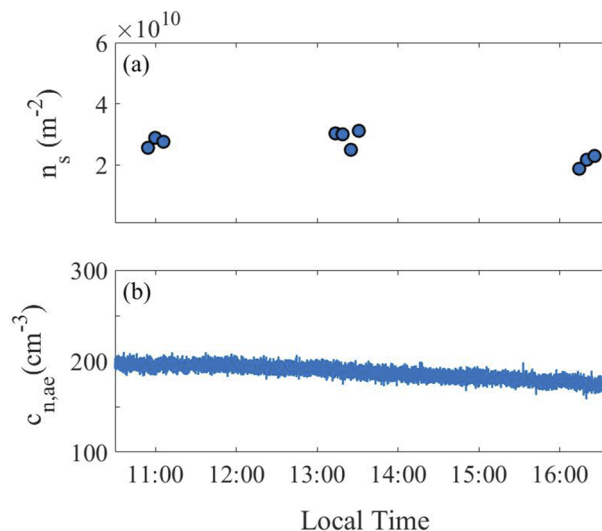


FIG. 5. INAS density (n_s) values measured in repeated AIDAm runs with an expansion flow of 9 L min^{-1} during three shorter time periods within the overall AIDA experiment duration of about 5 h [panel (a)]. (b) Aerosol number concentration $c_{n,ae}$ in AIDA during the same time period.

over a longer time, which allows performing long-term aerosol sampling experiments with instruments like AIDAm. The upper panel in Fig. 5 shows three blocks of repeated AIDAm runs, all of which showed n_s values between $2 \times 10^{10} \text{ m}^{-2}$ and $3 \times 10^{10} \text{ m}^{-2}$, implying that AIDAm delivers reproducible results for constant settings over a long measurement time.

B. Homogeneous freezing of supercooled water droplets

To test and validate the onset temperature for homogeneous freezing of supercooled water droplets measured with AIDAm, an experiment with AS particles as seed aerosol for cloud droplet formation was performed. The freezing temperature of cloud droplets is well known from previous studies (e.g., Benz *et al.*, 2005) and is also well formulated with classical nucleation theory (Pruppacher and Klett, 2010). AS was injected into AIDA as described in Sec. II D. Due to the increasing relative humidity during AIDA or AIDAm expansion runs, AS takes up water, deliquesces, and forms almost pure liquid cloud droplets that are then expected to freeze homogeneously at a temperature between -35 and -37°C . AIDAm measured the homogeneous freezing onset temperature in a series of 53 runs, which were done with different expansion flow settings between 5 and 10 L min^{-1} . In Fig. 6, one representative example is shown for each of the three run series with different expansion flow settings. The results are shown as normalized ice number concentrations $c_{n,ice,norm}$ plotted against T_{gas} , which is calculated by dividing the measured ice number concentration $c_{n,ice}$ for each temperature step by the maximum ice number concentration $c_{n,ice,max}$ measured during the respective experiment,

$$c_{n,ice,norm} = \frac{c_{n,ice}}{c_{n,ice,max}}. \quad (2)$$

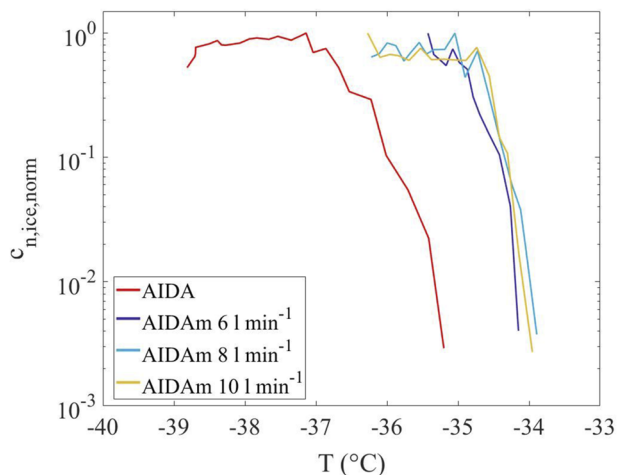


FIG. 6. Homogeneous freezing onset for supercooled water droplets measured with AIDA (red line) and AIDAm. The AIDAm expansions were performed with different expansion flow rate settings of 6, 8, and 10 L min⁻¹.

The homogeneous freezing onset is indicated by a steep increase in $c_{n,ice,norm}$ (Fig. 6), which occurred in AIDAm runs at $T_{gas} = -34.5^{\circ}\text{C}$ for all the probed expansion flows. This onset temperature is about 1.5°C higher compared to the literature and the result from the AIDA experiment (red line in Fig. 6). One explanation for this temperature offset may be related to the fact that the sensor measuring the lowest temperature in AIDAm is still located about 5 cm above the bottom of the chamber. Therefore, the expanding gas can be further cooled on the way to the OPC below the chamber and the minimum temperature of the aerosol can therefore be lower by about 1.5°C . Any further result is not corrected for this temperature offset of 1.5°C , but it will be considered for the uncertainties.

C. Homogeneous freezing and deposition nucleation at cirrus cloud temperatures

At temperatures below about -35°C , any ice formation in the atmosphere occurs either by homogeneous freezing of aqueous aerosol components or by heterogeneous ice-nucleation processes.

For the latter case, aerosol particles are needed to trigger the formation of ice crystals. In the atmosphere, aerosol particles are often transported over longer distances and longer time periods to the upper troposphere. During transport, the aerosol particles can undergo surface coating processes, which then possibly change their ice-nucleation ability and thereby their impact on cirrus cloud formation. Such coating processes can also influence the relative importance of homogeneous freezing and heterogeneous ice-nucleation processes during cirrus cloud formation.

In this section, we first demonstrate the capability of AIDAm to distinguish between homogeneous freezing and heterogeneous ice-nucleation at cirrus formation conditions, which is key to understand and quantify the relative contribution of the two ice-nucleation modes during the coating experiments that will be discussed in Sec. III D. The homogeneous freezing experiments were conducted with aerosol particles composed of an aqueous H_2SO_4 solution and the deposition ice-nucleation experiments were performed with SDSA_01 soil dust aerosol particles. All AIDA experiments and AIDAm runs discussed in this section were conducted at a start temperature of -45°C and AIDAm used the same expansion flow rates of 5 L min^{-1} . The AIDAm runs were then analyzed for the temporal change of the ice number concentration $c_{n,ice}$ at a one-second time resolution.

During the AIDAm homogeneous freezing runs [Fig. 7(a)], the measured $c_{n,ice}$ showed a steep increase in a short time interval around a run time of about 20 s. This is due to the steep increase of homogeneous freezing rates with decreasing temperature (Koop *et al.*, 2000) and is also observed in AIDA homogeneous freezing experiments (e.g., Schneider *et al.*, 2021b). Such a step-wise increase during the AIDA and AIDAm cloud expansion runs indicates the occurrence of homogeneous freezing.

A different freezing behavior is observed during the AIDAm runs with the SDSA_01 aerosol [Fig. 7(b)]. Ice started to form already at a run time of about 6 s, when the ice saturation ratio S_{ice} was still low. The ice crystal number concentration then steadily increased for a run time of about 15 s, caused by the heterogeneous ice-nucleation on the dust particle surfaces to occur over a wide range of S_{ice} , which increased during the expansion run. This behavior is characteristic of heterogeneous ice-nucleation like deposition nucleation or pore condensation and freezing and has also been observed in previous AIDA experiments with different

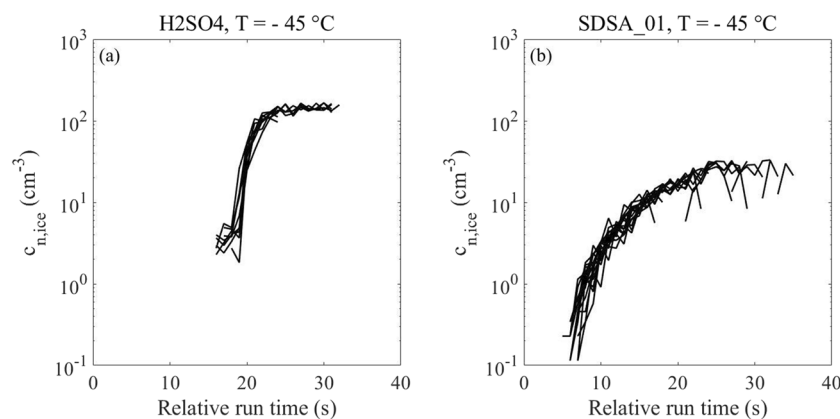


FIG. 7. Freezing behavior of aqueous H_2SO_4 particles (a) and the natural soil dust aerosol SDSA_01 (b), measured with AIDAm during 10 and 18 runs, respectively. The temperature in AIDAm at the start of the expansions was -45°C in both cases.

mineral dust aerosol types at cirrus cloud formation conditions (e.g., Möhler *et al.*, 2006).

The freezing curves from a series of 10 and 18 runs shown in Figs. 7(a) and 7(b), respectively, also document the high reproducibility of AIDAm experiments conducted at the same start temperature and expansion flow rate. The variability from run to run is rather low. This demonstrates that different freezing modes—like homogeneous freezing or deposition ice-nucleation—or a gradual shift from one mode to the other—e.g., during ongoing surface coating procedures—can well be identified and measured with AIDAm. The optimum expansion flow rate for AIDAm runs at cirrus formation temperatures was found to be 5 L min^{-1} . At this expansion flow rate, the steady increase in the ice number concentration with increasing S_{ice} was detected for a long time period after the start of the expansion [Fig. 7(a)] and the homogeneous freezing conditions were still reached well before the end of the expansion run [Fig. 7(a)]. A higher expansion flow rate would result in a higher increase rate of S_{ice} and a shorter run time to reach homogeneous freezing conditions, which would result in a reduced sensitivity and time resolution to detect heterogeneous ice formation. With a lower expansion flow rate, the homogeneous freezing conditions may not be reached anymore in an AIDAm run.

D. Long-term ice-nucleation measurements with AIDAm

The strength of AIDAm is its ability to continuously measure the ice-nucleating ability of aerosol sampled from AIDA over long time periods, hours to days, with a time resolution of up to 6 min. Thus, even small changes in the ice-nucleation behavior due to physical or chemical aging processes can be detected.

One such aging procedure is the coating of solid aerosol particles, such as dust, with gases like sulfuric acid. Previous laboratory ice-nucleation experiments have shown that surface coating can significantly change the ice-nucleation behavior of mineral dust particles at cirrus cloud temperatures (e.g., Knopf and Koop, 2006; Cziczo *et al.*, 2009). Most of these experiments have been conducted for a limited number of specific coating amounts or with coating layers generated at conditions far from those present during the atmospheric coating process. With AIDAm, it was possible to monitor the change in ice-nucleation behavior during the whole coating procedure of about 5 h, while the coating was performed inside AIDA at conditions representative of the atmosphere. The experiment was conducted as a proof-of-concept experiment, meaning that the aerosol residence time is not limited to the time in this study, but can be up to one week.

The coating experiment described here was conducted with SDSA_01, the same dust sample already used for the validation experiments discussed in Secs. III A and III C. The coating process of the pristine aerosol inside AIDA was induced and controlled by the chemical reaction of the precursor gases O_3 , SO_2 , and TME at a temperature of -45°C , thus, simulating typical tropospheric formation processes of the coating material H_2SO_4 . During the ongoing coating process, AIDAm performed 120 runs to continuously measure the ice-nucleation ability of the aerosol sampled from the AIDA chamber. Therefore, the combination of AIDA and AIDAm provides a unique opportunity for investigating the modification of the

ice-nucleation behavior of aerosols during ongoing coating processes typical for atmospheric aerosol transport conditions and for time scales of hours to days.

Figure 8 shows the timeline of a typical experiment of coating aerosols inside the AIDA chamber. At the beginning of an experiment, AIDAm is operated with particle-free air from AIDA for 15–30 min to measure the background conditions for ice crystal detection. Thereafter, a certain amount of dust aerosol is injected into the AIDA chamber. During the whole experimental procedure, the number concentration and the size distribution of the aerosol in the AIDA chamber are monitored with a time resolution of 1 s and 30–60 min, respectively. Right after the dust injection, AIDAm started to measure the aerosol ice-nucleation behavior as described in Sec. II B 2 in a series of runs with the same settings to obtain a consistent dataset throughout the experiment.

The ice-nucleation behavior of the non-coated aerosol is measured during the first 1.5–2 h. The first step of the coating procedure was the addition of O_3 following a similar procedure as described by Saathoff *et al.* (2009) to mainly check any background contamination in the AIDA chamber reacting with O_3 . The initial maximum O_3 concentration was about 700 ppb. After O_3 addition, the ice-nucleation activity was measured for about 30–60 min, before the volatile precursors SO_2 and TME were added. TME was added in amounts of 7–15 ppb to the AIDA chamber to generate, by reaction with O_3 , OH radicals, which then reacted with SO_2 to initiate the gas-phase formation of H_2SO_4 molecules. TME was added in small amounts about three or four times per hour, to slowly increase the coating amount over a longer time period. Because SO_2 is also lost to the chamber walls with a time constant of about 1 h, new portions of SO_2 were added to the AIDA chamber every hour. This caused a stepwise increase of the SO_2 concentration and, thereby, also a stepwise increase of the H_2SO_4 coating. The change in the ice-nucleation activity was measured with AIDAm during the coating process, which lasted for about 5 h.

The coating experiment was analyzed in the same way as the measurements discussed in Sec. III C. The time series of ice number concentrations measured in individual runs are depicted in Fig. 9(a) as solid lines with the color code for the time (in hours) relative to the start of the AIDAm runs. The ice onset for the non-coated aerosol (blue colors) occurs at about 5 s relative run time of the AIDAm run. The heterogeneous ice-nucleation activity observed before coating

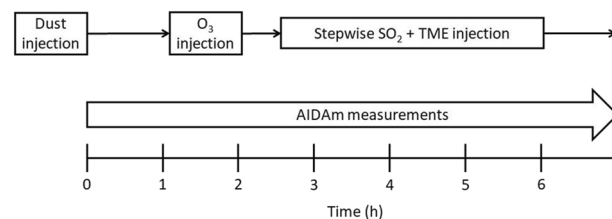


FIG. 8. Flowchart showing the typical experimental procedure of a coating experiment. The continuous AIDAm measurements started right after the dust aerosol injection. For the coating procedure, O_3 was added first, followed by adding tetramethylethylene (TME) several times per hour to form OH radicals by reaction with O_3 . The OH radicals then reacted with SO_2 to initiate the gas-phase formation of H_2SO_4 molecules.

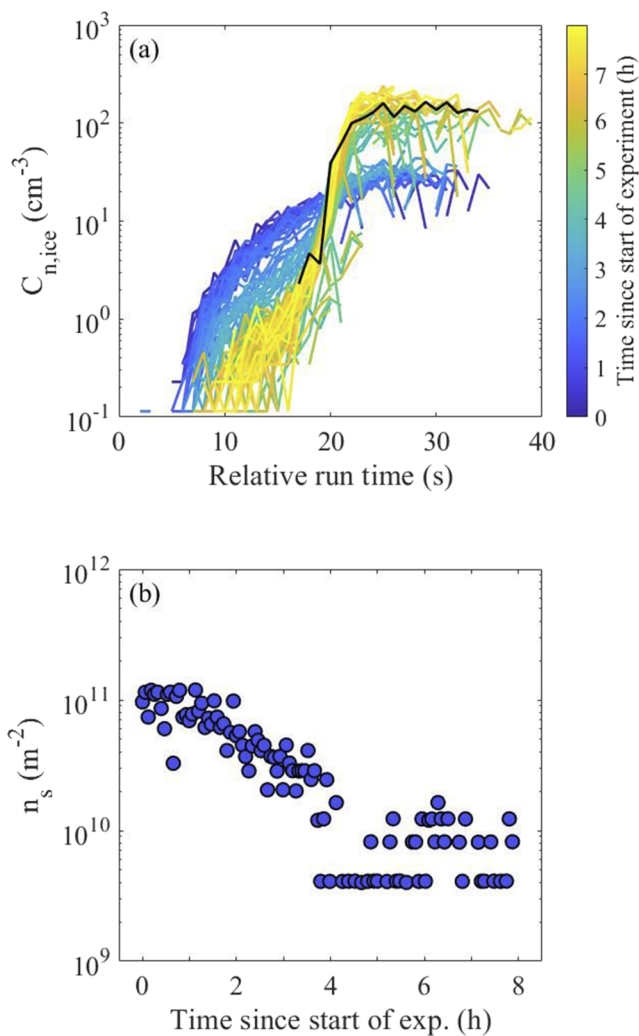


FIG. 9. Time series of the ice number concentrations plotted as a function of relative run time for all AIDA runs (a). The color code shows the experiment time in hours from when the AIDA runs were started. The AIDA temperature was set to -45°C . The blueish lines represent the AIDA runs with the non-coated dust aerosol sampled from AIDA and the greenish and yellowish lines the AIDA runs with the coated aerosol. The solid black line shows one representative AIDA run for homogeneous freezing of aqueous H_2SO_4 aerosols [Fig. 7(a)]. The solid black line in the color bar indicates the O_3 injection, and the dashed line the start of the coating procedure. (b) Calculated n_s for every AIDA run at a relative run time of 15 s.

well agrees with the experiment shown in Fig. 7(b), highlighting the high repeatability of AIDA measurements for the same aerosol.

The ice saturation ratio S_{ice} is increasing in the course of an AIDA expansion run as explained in Sec. III C and also shown in Fig. 11 in Appendix A 2. With a linear fit between ice saturated conditions ($S_{\text{ice}} = 1.0$) at the start of the expansion and $S_{\text{ice}} = 1.38$ at a run time of 20 s, the homogeneous freezing onset during AIDA runs, that started at a temperature of -45°C (see Sec. III C), the ice saturation ratio is about 1.1 after 5 s run time when heterogeneous ice-nucleation was observed to start for the non-coated aerosols.

Ozone was added to the aerosol in AIDA at an experiment time of 1.3 h, indicated by a solid black line in the color bar of Fig. 9. The $c_{n,\text{ice}}$ curves did not change after ozone addition, which means that the ozone alone did not affect the aerosol ice-nucleation activity. The coating procedure started at an experiment time of 2.0 h, indicated by a dashed black line in the color bar of Fig. 9. During the coating with H_2SO_4 (transition to green and yellow colors), the ice formation onset was shifted toward later run times, but the shape of the curves remained almost the same (greenish colors and experiment times up to 5 h). From this, we can conclude that thin coating layers suppressed the deposition ice-nucleation activity of these aerosols at low S_{ice} and shifted the onset of heterogeneous ice formation to higher S_{ice} values.

The coating-induced reduction of ice-nucleation activity is also presented in Fig. 9(b), which shows the time series of n_s calculated for each AIDA run at a relative run time of 15 s. The n_s is a measure for the ice-nucleation activity of the aerosol particles per particle surface area. For the experiments, the n_s decreased by about one order of magnitude during the first 3 h of coating time, from about $1 \times 10^{11} \text{ m}^{-2}$ for the non-coated aerosols to about $1 \times 10^{10} \text{ m}^{-2}$ for the coated aerosols.

After about 5 h experiment time, the shape of the $c_{n,\text{ice}}$ curves was found to be clearly changing. A second steep increase in the ice number concentration occurred at a run time of about 20 s, which is the time when homogeneous freezing was observed with AIDA in experiments with pure aqueous H_2SO_4 aerosol particles [Fig. 7(a)]. One representative $c_{n,\text{ice}}$ curve measured with AIDA during the homogeneous freezing experiments is shown as a solid black line in Fig. 9. This surface coating-induced change in the ice-nucleation behavior is caused by an increasing contribution of homogeneous freezing of the coating layer to the overall ice-nucleation activity of the aerosol, while the contribution from heterogeneous ice-nucleation at the surface of the solid dust aerosol particles is reduced by the coating layer.

IV. SUMMARY

AIDA is a new cloud expansion chamber of 20 L volume developed for lab-based aerosol–cloud process studies with a high time resolution of minutes and automated long-term measurement series of INPs over hours or days. It is mounted inside the thermal housing of the well-established AIDA cloud expansion chamber (e.g., Möhler *et al.*, 2003; 2006) and is directly connected to it with a straight vertical sampling line. Therefore, it can sample aerosol particles over a wide size range directly from the AIDA chamber, which serves not only as a long-term reservoir of atmospherically relevant aerosol particles but also as a place for dedicated physical and chemical modification of the aerosol particles under well-controlled temperature, pressure, and humidity conditions. Aerosol processing and ice-nucleation experiments in AIDA and AIDA can be conducted over a wide temperature range from about -5 to -90°C , which covers the range of both mixed-phase and cirrus cloud formation conditions.

The operation principle of AIDA is similar to that of the recently developed Portable Ice Nucleation Experiment, PINE (Möhler *et al.*, 2021). The operation is based on a series of runs that are composed of three modes: flush mode, expansion mode, and refill mode. During the flush mode, the cloud chamber is flushed

with air from AIDA containing the aerosol under investigation. During the expansion mode, the aerosol in the AIDAm cloud chamber is expanded in order to activate the sampled aerosol particles as cloud condensation nuclei and ice-nucleating particles. During the refill mode, the cloud chamber is refilled until the initial pressure conditions are reached. A single run takes about 6 min and can be repeated with automated control over long time periods of hours or days.

The new AIDAm instrument was tested and validated for experiments on immersion freezing of soil dust aerosol particles at mixed-phase cloud temperatures, homogeneous freezing of cloud water droplets, and heterogeneous and homogeneous ice formation processes relevant for cirrus clouds. The experiments on immersion freezing were analyzed for the temperature-dependent INAS density (n_s), which is a parameter related to the ice-nucleation activity per aerosol surface area (e.g., Niemand *et al.*, 2012; Ullrich *et al.*, 2017). The n_s measured with AIDAm showed good agreement with the results from the AIDA cloud chamber experiments and the INSEKT method only for expansion flow rates close to 10 L min⁻¹. At lower expansion flow rates, the AIDAm results showed an increasing low bias compared to the other methods, with a difference of up to one order of magnitude at an expansion flow rate of 7 L min⁻¹. The reason for this discrepancy could be the incomplete activation of aerosol particles to supercooled cloud droplets at lower expansion rates inside the AIDAm chamber. At higher expansion flow rates, n_s for immersion freezing of dust aerosols was measured with low variability in repeated runs over several hours. This showed that AIDAm ice-nucleation measurements are reproducible in repeated runs with identical run parameters and slight changes in the ice-nucleation activity, e.g., since surface coating can be detected with AIDAm. The onset temperature for homogeneous freezing of solution droplets was measured with AIDAm at temperatures between -34 and -35 °C, independent of the expansion flow rate. The observed freezing temperature is about 1.5 °C higher compared to AIDA, which may be caused by a somewhat larger temperature non-homogeneity in the much smaller AIDAm chamber during the expansion. The AIDAm measurements at cirrus cloud temperatures revealed that heterogeneous ice formation on mineral dust aerosols can clearly be distinguished from homogeneous freezing of sulfuric acid solution particles when looking into the rate of ice crystal detection with expansion time and the onset time of ice formation after the start time of the expansion. The time of ice onset is closely related to the ice supersaturation of ice formation.

A 7 h long experiment deploying the new combination of AIDAm and AIDA cloud simulation chambers was used to show the possibilities of AIDAm to monitor changes in the ice-nucleation activity of the aerosol in AIDA over long time periods. Therefore, dust aerosol particles in AIDA were slowly coated with sulfuric acid, while AIDAm was continuously sampling the aerosol for ice nucleation measurements. The experiment was carried out at a temperature of -45 °C, where it was known from previous work that a change in the ice-nucleating activity can be expected. A clear transition was observed from deposition nucleation behavior to homogeneous freezing. The deposition nucleation behavior is characterized by an early ice formation onset at low ice supersaturation in the AIDAm chamber, followed by a steady increase in ice crystal formation over a longer time period of the

expansion run. The homogeneous freezing behavior is characterized by a later ice formation onset followed by a steep increase in ice crystal formation. Toward the end of the coating period, the ice formation curves agreed well with those measured for pure sulfuric acid solution aerosols.

In this study, we introduced the working principle of the newly developed AIDAm cloud expansion chamber. The validation experiments and results were aimed at underlining the strength of combining the AIDAm cloud expansion chamber with the well-established AIDA cloud simulation chamber for performing dedicated laboratory experiments on aerosol–cloud interaction processes at simulated atmospheric conditions, including long-term processes like surface coating, which occur during long-range transport of atmospheric aerosol particles and modify their chemical composition and physical properties, such as their ability to act as ice-nucleating particles in clouds. Future experiments with the new combinations of the AIDA and AIDAm cloud simulation chambers will be conducted over even longer time periods of up to one week, to simulate atmospheric aerosol aging processes, especially at higher altitudes and latitudes. Such experiments also simulate the aging of aerosol particles due to radiation simulated by a light source inside AIDA, which represents the solar spectrum (Vallon *et al.*, 2022). Moreover, experiments conducted over days starting with high dust aerosol concentrations in AIDA are expected show a potential impact of the coagulation of two solid particles on heterogeneous ice formation.

ACKNOWLEDGMENTS

We thank the AIDA technical team for their continuous help and support during the AIDA campaigns.

AUTHOR DECLARATIONS

Conflict of Interest

The authors have no conflicts to disclose.

Author Contributions

F.V. set up the instrument, performed the measurements, and analyzed the data. J.N. wrote the control software for the instrument. F.V., L.L., H.S., T.L., and O.M. contributed to the discussion and interpretation of the data. F.V. and O.M. prepared the manuscript.

F. Vogel: Conceptualization (equal); Formal analysis (equal); Validation (equal); Visualization (equal); Writing – original draft (equal); Writing – review & editing (equal). **L. Lacher:** Supervision (supporting); Writing – review & editing (supporting). **J. Nadolny:** Conceptualization (supporting); Software (lead). **H. Saathoff:** Investigation (supporting); Writing – review & editing (supporting). **T. Leisner:** Resources (supporting); Supervision (supporting); Writing – review & editing (supporting). **O. Möhler:** Conceptualization (equal); Investigation (equal); Supervision (equal); Validation (equal); Writing – original draft (equal); Writing – review & editing (equal).

DATA AVAILABILITY

The data that support the findings of this study are available from the corresponding author upon reasonable request.

APPENDIX: TEMPERATURE AND SATURATION CALCULATIONS FOR AIDAm

1. Temperature calibration for AIDAm

AIDAm is located in the AIDA cold box with a homogeneous temperature control. The temperature in this box is measured with thermocouples that are calibrated against a reference sensor with an accuracy of ± 0.1 °C. Figure 10 shows the uncorrected reading of the AIDAm temperature (T_{gas} , red symbols) compared to the AIDA cold box temperature in the temperature range from -21 to -60 °C. From these data, a calibration function (polynomial fit of third order) given by

$$T_{\text{gas,corr}} = T_{\text{gas}} + (0.000\,122\,7 \cdot T_{\text{gas}}^3 + 0.013\,76 \cdot T_{\text{gas}}^2 + 0.5308 \cdot T_{\text{gas}} + 4.067) \quad (\text{A1})$$

was derived for the AIDAm temperature sensors. The calibrated temperatures ($T_{\text{gas,corr}}$) are shown as yellow symbols in Fig. 10.

2. Calculation of S_{ice}

The setup of AIDAm has no instrument included to directly measure the humidity in the chamber, but an estimate for the S_{ice} value during an expansion is given here. At the beginning of an expansion, it is assumed that S_{ice} is at saturated conditions and therefore has a value of 1. During the course of an experiment, S_{ice} increases linearly and, without the presence of ice-nucleating particles, reaches the values for homogeneous freezing. From the experiment performed with the pure H_2SO_4 solutes, it is known that homogeneous freezing is observed after 20 and 23 s of relative run time for -45 and -55 °C, respectively. The corresponding S_{ice} values are calculated following the latest parameterization for homogeneous freezing (Schneider *et al.*, 2021b). The calculation presented in Fig. 11 is only valid for the experiments at cirrus cloud conditions made with a flow of 5 L min^{-1} .

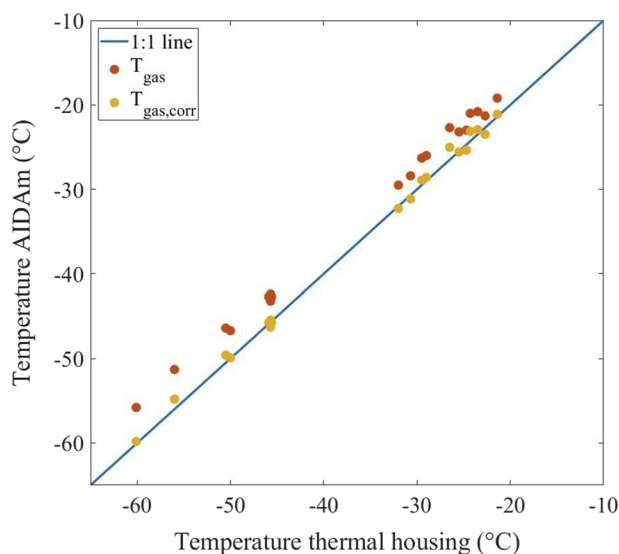


FIG. 10. Raw (red symbols) and calibrated (yellow symbols) temperatures in AIDAm, compared to the AIDA cold box temperature.

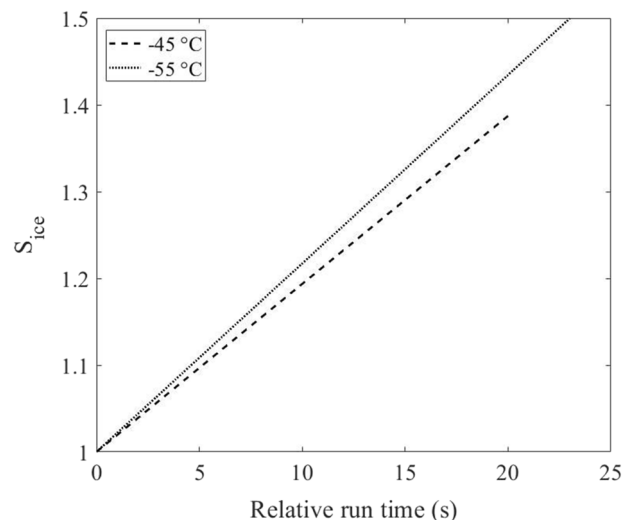


FIG. 11. Linear fit of the saturation condition with respect to ice (S_{ice}) for the experiments performed at -45 °C (dashed line) and -55 °C (solid line).

REFERENCES

- Atkinson, J. D., Murray, B. J., Woodhouse, M. T., Whale, T. F., Baustian, K. J., Carslaw, K. S., Dobbie, S., O'Sullivan, D., and Malkin, T. L., "The importance of feldspar for ice nucleation by mineral dust in mixed-phase clouds," *Nature* **498**, 355–358 (2013).
- Benz, S., Megahed, K., Möhler, O., Saathoff, H., Wagner, R., and Schurath, U., "T-dependent rate measurements of homogeneous ice nucleation in cloud droplets using a large atmospheric simulation chamber," *J. Photochem. Photobiol., A* **176**, 208–217 (2005), in Honour of Professor Richard P. Wayne.
- Betzner, P. R., Carder, K. L., Duce, R. A., Merrill, J. T., Tindale, N. W., Uematsu, M., Costello, D. K., Young, R. W., Feely, R. A., Breland, J. A., Bernstein, R. E., and Greco, A. M., "Long-range transport of giant mineral aerosol particles," *Nature* **336**, 568–571 (1988).
- Boose, Y., Baloh, P., Plötze, M., Ofner, J., Grothe, H., Sierau, B., Lohmann, U., and Kanji, Z. A., "Heterogeneous ice nucleation on dust particles sourced from nine deserts worldwide—Part 2: Deposition nucleation and condensation freezing," *Atmos. Chem. Phys.* **19**, 1059–1076 (2019).
- Chang, K., Bench, J., Brege, M., Cantrell, W., Chandrakar, K., Ciochetto, D., Mazzoleni, C., Mazzoleni, L. R., Niedermeier, D., and Shaw, R. A., "A laboratory facility to study gas-aerosol-cloud interactions in a turbulent environment: The π chamber," *Bull. Am. Meteorol. Soc.* **97**, 2343–2358 (2016).
- Chou, C., Stetzer, O., Weingartner, E., Jurányi, Z., Kanji, Z. A., and Lohmann, U., "Ice nuclei properties within a Saharan dust event at the Jungfraujoch in the Swiss Alps," *Atmos. Chem. Phys.* **11**, 4725–4738 (2011).
- Cziczo, D. J., Froyd, K. D., Gallavardin, S. J., Moehler, O., Benz, S., Saathoff, H., and Murphy, D. M., "Deactivation of ice nuclei due to atmospherically relevant surface coatings," *Environ. Res. Lett.* **4**, 044013 (2009).
- David, R. O., Marcolli, C., Fahrni, J., Qiu, Y., Perez Sirkin, Y. A., Molinero, V., Mahrt, F., Brühwiler, D., Lohmann, U., and Kanji, Z. A., "Pore condensation and freezing is responsible for ice formation below water saturation for porous particles," *Proc. Natl. Acad. Sci. U. S. A.* **116**, 8184–8189 (2019).
- de Boer, G., Morrison, H., Shupe, M. D., and Hildner, R., "Evidence of liquid dependent ice nucleation in high-latitude stratiform clouds from surface remote sensors," *Geophys. Res. Lett.* **38**, L01803, <https://doi.org/10.1029/2010GL046016> (2011).
- Fahy, D. W., Gao, R.-S., Möhler, O., Saathoff, H., Schiller, C., Ebert, V., Krämer, M., Peter, T., Amarouche, N., Avallone, L. M., Bauer, R., Bozóki, Z., Christensen, L. E., Davis, S. M., Durre, G., Dyrhoff, C., Herman, R. L., Hunsmann, S., Khaykin, S. M., Mackrodt, P., Meyer, J., Smith, J. B., Spelten,

- N., Troy, R. F., Vömel, H., Wagner, S., and Wienhold, F. G., "The aquavit-1 intercomparison of atmospheric water vapor measurement techniques," *Atmos. Meas. Tech.* **7**, 3177–3213 (2014).
- Hinds, W. C., *Aerosol Technology: Properties, Behavior, and Measurement of Airborne Particles* (John Wiley & Sons, 2012).
- Hiranuma, N., Augustin-Bauditz, S., Bingemer, H., Budke, C., Curtius, J., Danielczok, A., Diehl, K., Dreischmeier, K., Ebert, M., Frank, F., Hoffmann, N., Kandler, K., Kiselev, A., Koop, T., Leisner, T., Möhler, O., Nillius, B., Peckhaus, A., Rose, D., Weinbruch, S., Wex, H., Boose, Y., DeMott, P. J., Hader, J. D., Hill, T. C. J., Kanji, Z. A., Kulkarni, G., Levin, E. J. T., McCluskey, C. S., Murakami, M., Murray, B. J., Niedermeier, D., Petters, M. D., O'Sullivan, D., Saito, A., Schill, G. P., Tajiri, T., Tolbert, M. A., Welti, A., Whale, T. F., Wright, T. P., and Yamashita, K., "A comprehensive laboratory study on the immersion freezing behavior of illite NX particles: A comparison of 17 ice nucleation measurement techniques," *Atmos. Chem. Phys.* **15**, 2489–2518 (2015).
- Hoose, C. and Möhler, O., "Heterogeneous ice nucleation on atmospheric aerosols: A review of results from laboratory experiments," *Atmos. Chem. Phys.* **12**, 9817–9854 (2012).
- Ignatius, K., Kristensen, T. B., Järvinen, E., Nichman, L., Fuchs, C., Gordon, H., Herenz, P., Hoyle, C. R., Duplissy, J., Garimella, S., Dias, A., Frege, C., Höppel, N., Tröstl, J., Wagner, R., Yan, C., Amorim, A., Baltensperger, U., Curtius, J., Donahue, N. M., Gallagher, M. W., Kirkby, J., Kulmala, M., Möhler, O., Saathoff, H., Schnaiter, M., Tomé, A., Virtanen, A., Worsnop, D., and Stratmann, F., "Heterogeneous ice nucleation of viscous secondary organic aerosol produced from ozonolysis of α -pinene," *Atmos. Chem. Phys.* **16**, 6495–6509 (2016).
- Järvinen, E., Vochezer, P., Möhler, O., and Schnaiter, M., "Laboratory study of microphysical and scattering properties of corona-producing cirrus clouds," *Appl. Opt.* **53**, 7566–7575 (2014).
- Kanji, Z. A., Ladino, L. A., Wex, H., Boose, Y., Burkert-Kohn, M., Cziczko, D. J., and Krämer, M., "Overview of ice nucleating particles," *Meteorol. Monogr.* **58**, 1.1–1.33 (2017).
- Knippertz, P. and Todd, M. C., "Mineral dust aerosols over the Sahara: Meteorological controls on emission and transport and implications for modeling," *Rev. Geophys.* **50**, RG1007, <https://doi.org/10.1029/2011RG000362> (2012)
- Knopf, D. A. and Koop, T., "Heterogeneous nucleation of ice on surrogates of mineral dust," *J. Geophys. Res.: Atmos.* **111**, D12201, <https://doi.org/10.1029/2005JD006894> (2006).
- Koop, T., Luo, B., Tsias, A., and Peter, T., "Water activity as the determinant for homogeneous ice nucleation in aqueous solutions," *Nature* **406**, 611–614 (2000).
- Maier, S., Tamm, A., Wu, D., Caesar, J., Grube, M., and Weber, B., "Photoautotrophic organisms control microbial abundance, diversity, and physiology in different types of biological soil crusts," *ISME J.* **12**, 1032–1046 (2018).
- Marcollì, C., "Technical note: Fundamental aspects of ice nucleation via pore condensation and freezing including Laplace pressure and growth into macroscopic ice," *Atmos. Chem. Phys.* **20**, 3209–3230 (2020).
- Möhler, O., Adams, M., Lacher, L., Vogel, F., Nadolny, J., Ullrich, R., Boffo, C., Pfeuffer, T., Hobl, A., Weiß, M., Vepuri, H. S. K., Hiranuma, N., and Murray, B. J., "The portable ice nucleation experiment (pine): A new online instrument for laboratory studies and automated long-term field observations of ice-nucleating particles," *Atmos. Meas. Tech.* **14**, 1143–1166 (2021).
- Möhler, O., Benz, S., Saathoff, H., Schnaiter, M., Wagner, R., Schneider, J., Walter, S., Ebert, V., and Wagner, S., "The effect of organic coating on the heterogeneous ice nucleation efficiency of mineral dust aerosols," *Environ. Res. Lett.* **3**, 025007 (2008).
- Möhler, O., Field, P. R., Connolly, P., Benz, S., Saathoff, H., Schnaiter, M., Wagner, R., Cotton, R., Krämer, M., Mangold, A., and Heymsfield, A. J., "Efficiency of the deposition mode ice nucleation on mineral dust particles," *Atmos. Chem. Phys.* **6**, 3007–3021 (2006).
- Möhler, O., Stetzer, O., Schaefers, S., Linke, C., Schnaiter, M., Tiede, R., Saathoff, H., Krämer, M., Mangold, A., Budz, P., Zink, P., Schreiner, J., Mauersberger, K., Haag, W., Kärcher, B., and Schurath, U., "Experimental investigation of homogeneous freezing of sulphuric acid particles in the aerosol chamber AIDA," *Atmos. Chem. Phys.* **3**, 211–223 (2003).
- Murray, B. J., O'Sullivan, D., Atkinson, J. D., and Webb, M. E., "Ice nucleation by particles immersed in supercooled cloud droplets," *Chem. Soc. Rev.* **41**, 6519–6554 (2012).
- Niemand, M., Möhler, O., Vogel, B., Vogel, H., Hoose, C., Connolly, P., Klein, H., Bingemer, H., DeMott, P., Skrotzki, J., and Leisner, T., "A particle-surface-area-based parameterization of immersion freezing on desert dust particles," *J. Atmos. Sci.* **69**, 3077–3092 (2012).
- Pruppacher, H. and Klett, J., *Microphysics of Clouds and Precipitation, Atmospheric and Oceanographic Sciences Library* (Springer Netherlands, 2010).
- Saathoff, H., Naumann, K.-H., Riemer, N., Kamm, S., Möhler, O., Schurath, U., Vogel, H., and Vogel, B., "The loss of NO₂, HNO₃, NO₃/N₂O₅, and HO₂/HOONO₂ on soot aerosol: A chamber and modeling study," *Geophys. Res. Lett.* **28**, 1957–1960, <https://doi.org/10.1029/2000gl012619> (2001).
- Saathoff, H., Naumann, K.-H., Schnaiter, M., Schöck, W., Möhler, O., Schurath, U., Weingartner, E., Gysel, M., and Baltensperger, U., "Coating of soot and (NH₄)₂SO₄ particles by ozonolysis products of α -pinene," *J. Aerosol Sci.* **34**, 1297–1321 (2003), intercomparison of Soot Measurement Techniques.
- Saathoff, H., Naumann, K.-H., Möhler, O., Jonsson, Å. M., Hallquist, M., Kiendler-Scharr, A., Mentel, T. F., Tillmann, R., and Schurath, U., "Temperature dependence of yields of secondary organic aerosols from the ozonolysis of α -pinene and limonene," *Atmos. Chem. Phys.* **9**, 1551–1577 (2009).
- Schnaiter, M., Linke, C., Möhler, O., Naumann, K.-H., Saathoff, H., Wagner, R., Schurath, U., and Wehner, B., "Absorption amplification of black carbon internally mixed with secondary organic aerosol," *J. Geophys. Res.: Atmos.* **110**, D19204, <https://doi.org/10.1029/2005JD006046> (2005).
- Schneider, J., Höhler, K., Heikkilä, P., Keskinen, J., Bertozzi, B., Bogert, P., Schorr, T., Umo, N. S., Vogel, F., Brasseur, Z., Wu, Y., Hakala, S., Duplissy, J., Moiseev, D., Kulmala, M., Adams, M. P., Murray, B. J., Korhonen, K., Hao, L., Thomson, E. S., Castarède, D., Leisner, T., Petäjä, T., and Möhler, O., "The seasonal cycle of ice-nucleating particles linked to the abundance of biogenic aerosol in boreal forests," *Atmos. Chem. Phys.* **21**, 3899–3918 (2021a).
- Schneider, J., Höhler, K., Wagner, R., Saathoff, H., Schnaiter, M., Schorr, T., Steinke, I., Benz, S., Baumgartner, M., Rolf, C., Krämer, M., Leisner, T., and Möhler, O., "High homogeneous freezing onsets of sulfuric acid aerosol at cirrus temperatures," *Atmos. Chem. Phys. Discuss.* **21**, 14403–14425 (2021b).
- Seinfeld, J. H. and Pandis, S. N., *Atmospheric Chemistry and Physics: From Air Pollution to Climate Change* (John Wiley & Sons, 2016).
- Ullrich, R., Hoose, C., Möhler, O., Niemand, M., Wagner, R., Höhler, K., Hiranuma, N., Saathoff, H., and Leisner, T., "A new ice nucleation active site parameterization for desert dust and soot," *J. Atmos. Sci.* **74**, 699–717 (2017).
- Vali, G., "Quantitative evaluation of experimental results on the heterogeneous freezing nucleation of supercooled liquids," *J. Atmos. Sci.* **28**, 402–409 (1971).
- Vali, G., DeMott, P. J., Möhler, O., and Whale, T. F., "Technical note: A proposal for ice nucleation terminology," *Atmos. Chem. Phys.* **15**, 10263–10270 (2015).
- Vallon, M., Gao, L., Jiang, F., Krumm, B., Nadolny, J., Song, J., Leisner, T., and Saathoff, H., "Led-based solar simulator to study photochemistry over a wide temperature range in the large simulation chamber aida," *Atmos. Meas. Tech.* **15**, 1795–1810 (2022).
- Wagner, R., Benz, S., Möhler, O., Saathoff, H., and Schurath, U., "Probing ice clouds by broadband mid-infrared extinction spectroscopy: Case studies from ice nucleation experiments in the AIDA aerosol and cloud chamber," *Atmos. Chem. Phys.* **6**, 4775–4800 (2006).
- Wagner, R., Kiselev, A., Möhler, O., Saathoff, H., and Steinke, I., "Pre-activation of ice-nucleating particles by the pore condensation and freezing mechanism," *Atmos. Chem. Phys.* **16**, 2025–2042 (2016).
- Weinzierl, B., Ansmann, A., Prospero, J. M., Althausen, D., Benker, N., Chouza, F., Dollner, M., Farrell, D., Fomba, W. K., Freudenthaler, V., Gasteiger, J., Groß, S., Haarig, M., Heinold, B., Kandler, K., Kristensen, T. B., Mayol-Bracero,

- O. L., Müller, T., Reitebuch, O., Sauer, D., Schäfler, A., Schepanski, K., Spanu, A., Tegen, I., Toledano, C., and Walser, A., "The saharan aerosol long-range transport and aerosol–cloud-interaction experiment: Overview and selected highlights," *Bull. Am. Meteorol. Soc.* **98**, 1427–1451 (2017).
- Wex, H., Augustin-Bauditz, S., Boose, Y., Budke, C., Curtius, J., Diehl, K., Dreyer, A., Frank, F., Hartmann, S., Hiranuma, N., Jantsch, E., Kanji, Z. A., Kiselev, A., Koop, T., Möhler, O., Niedermeier, D., Nillius, B., Rösch, M., Rose, D., Schmidt, C., Steinke, I., and Stratmann, F., "Intercomparing different devices for the investigation of ice nucleating particles using Snomax[®] as test substance," *Atmos. Chem. Phys.* **15**, 1463–1485 (2015).
- Wolf, M. J., Zhang, Y., Zawadowicz, M. A., Goodell, M., Froyd, K., Freney, E., Sellegri, K., Rösch, M., Cui, T., Winter, M., Lacher, L., Axisa, D., DeMott, P. J., Levin, E. J. T., Gute, E., Abbatt, J., Koss, A., Kroll, J. H., Surratt, J. D., and Cziczo, D. J., "A biogenic secondary organic aerosol source of cirrus ice nucleating particles," *Nat. Commun.* **11**, 4834 (2020).